13 (2023) 100309

Contents lists available at ScienceDirect

Biosensors and Bioelectronics: X

journal homepage: www.journals.elsevier.com/biosensors-and-bioelectronics-x

Silver-coated ZnO disordered nanostructures as low-cost and label-free Raman biosensing platform for fast detection of complex organic profiles

L. Maiolo [a], F. Maita [a,*], J.I. Del Rio De Vicente [a], I. Lucarini [a], G. Strisciullo [b], S. Sablone [b], A. Liscio [a], G. Petrone [a], V. Mussi [a]

[a] Istituto per la Microelettronica e i Microsistemi, Consiglio Nazionale delle Ricerche, Via del Fosso del Cavaliere n.100, 00133, Roma, Italy
[b] Section of Legal Medicine, Interdisciplinary Department of Medicine, Bari Policlinico Hospital, University of Bari, Piazza Giulio Cesare 11, 70124, Bari, Italy

ARTICLE INFO

Keywords:
ZnO nanostructures
Excimer laser annealing
Raman spectroscopy
Rhodamine
Human blood

ABSTRACT

The need of cheap and easy to use biosensors for rapid diagnostics is a crucial challenge in medicine: indeed, devices must offer multiple properties such as fast response, high sensitivity, reduced need of sample processing, etc. In this respect, optical biosensors remain a promising class of biodevices. Here we present an extensive investigation of the surface properties of silver-coated zinc oxide disordered nanostructures as efficient biosensing platform to detect complex organic profiles via Raman spectroscopy. In particular, we combine low temperature and large area manufacturing techniques to offer a low-cost tool for rapid detection of untreated organic samples like human blood avoiding the usage of expensive manufacturing methods to grow ordered nanostructures and providing safer materials respect the implementation of metal nanoparticles thus opening the possibility to adopt these devices also in vivo. After an accurate study using rhodamine, comparing Raman response for as deposited and lasered surfaces, different metal layers (gold vs silver) and different metal thicknesses (from 25 to 150 nm), we successfully validate the performance of the silver-coated lasered platform on untreated human blood obtaining high resolved response and identifying several organic signatures attributable to hypoxanthine, glucose and lipoprotein.

1. Introduction

The identification of effective manufacturing methods to fabricate low-cost, label free and sustainable biosensors for a rapid diagnostics of complex organic samples remains a challenging task. Indeed, if miniaturization and implementation of nanoscience are offering intriguing opportunities to create biosensing platforms with extremely high sensitivity [Daima et al., 2020; Syedmoradi et al., 2017], a reasonable trade off must be always considered among device performance, manufacturing methods, promotion of environmental friendly materials and ease of use. Until now, although many diagnostic methodologies offer very precise response like polymerase chain reactions (PCRs), these technologies are time consuming and need skilled personnel to avoid sample contamination and make a correct data interpretation [Kuslich et al., 2018]. To obtain simple and fast detection, optical biosensors represent a promising class of devices deeply utilized in medicine from genomics to proteomics [Leonardi et al., 2018; Hakimian et al., 2018; Williams et al., 2018] due to the possibility of obtaining significant information also from complex organic samples. Among different techniques, Raman spectroscopy can offer signal amplification via interaction with nanometric metallic structures. This well-known phenomenon is called surface-enhanced Raman scattering (SERS) and can be a valuable ally for designing simple and effective tools for rapid diagnostics in medicine. SERS dates back to 70' and provides a molecular fingerprint of samples, also in liquid, exploiting the electromagnetic interaction of a laser with the metal nanostructured platform and the chemical/mechanical interaction of the samples with the 3D/2D surface of the device. During the years, the usage of metal nanoparticles (NPs) (in particular Au and Ag) to enhance the Raman response has been demonstrated as an effective strategy. NPs have been arranged on flat surface or on 3D nanostructures with interesting results [Seo et al., 2018; Mei et al., 2018; Mai et al., 2022; Tran et al., 2022], but an important drawback of this technology is the great dependency of the plasmon resonance by the size and the spacing of NPs; moreover, especially in vivo, the treatment can represent a health hazard for their accumulation in diverse organs like liver and kidneys [Tang et al., 2009; Korani et al.,

* Corresponding author.
E-mail address: francesco.maita@cnr.it (F. Maita).

https://doi.org/10.1016/j.biosx.2023.100309
Received 10 November 2022; Received in revised form 16 January 2023; Accepted 23 January 2023
Available online 4 February 2023

2015]. For these reasons, ad hoc tridimensional nanostructures can be preferred: in fact, even if the Raman response does not reach the performance of NPs, 3D nanostructured substrates can provide sufficient Raman amplification (SERS-like) to observe molecular fingerprint of organic samples exploiting both ordered or disordered configurations. While the manufacturing of ordered nanostructures usually requires expensive equipment (e.g. Electron beam lithography), disordered configurations can be successfully implemented using low-cost fabrication methods [Convertino et al., 2016; Lee and Choi, 2019; Raveendran et al., 2020]. In this respect, many different materials have been proposed, such as metal coated silicon nanowires, titanium oxide nanorods, tunable nanoporous copper, metal coated polymeric scaffold, etc. [Li et al., 2019; Chen et al., 2009; Tan et al., 2012]. While several materials are expensive in terms of deposition techniques or fabrication strategies, and others present severe issues with their environmental impact, a good candidate is zinc oxide (ZnO), since it shows a large variety of different nanostructures that can be obtained with low-cost manufacturing processes (e.g. chemical bath deposition), it is a non-toxic, easy to recycle, and it has well-known optical and electrical properties [Adesoye et al., 2022]. Several examples of these structures, implemented as SERS tool, have been reported exploiting ZnO nanorods decorated with silver NPs or graphene/Ag nano-resonators [Araujo et al., 2017; Huang et al., 2015; Zhu et al., 2019; Sun et al., 2020; Barveen et al., 2021]. Additionally, metallic zinc has been proposed as substitute of the metallic silver to further increase the green impact of the manufacturing process of these Raman platform [Proniewicz et al., 2020]. Regarding these 3D nanostructures, particular attention must be paid in tailoring a suitable morphology of the surface to maximize the Raman response: indeed, if the usage of metallic NPs does not allow a precise control of their distribution in size and shape as decoration along the nanostructures, different large area techniques can be implemented to increase the uniformity of the surface roughness of the Raman platform, crucial to demonstrate a useful reproducibility of the device (e.g. treatment in quartz oven or rapid thermal annealing). Unfortunately, the majority of these processes involves the heating of samples at high temperature (typically above 500 °C), precluding the possibility to integrate enhanced Raman biosensing platform on flexible and polymeric substrates. However, laser annealing can be used to locally heat the samples without affecting the mechanical properties on underlying flexible substrate: indeed, excimer laser annealing can provide sufficient energy to partially melt the nanostructures in a fast and safe way [Privitera et al., 2008; Fiaschi et al., 2018]. Excimer laser technique is a well-known strategy to treat recrystallization of semiconductors on polymeric foil [Pecora et al., 2008]. The laser pulse, in the range of nanosecond, can locally raise the temperature and a buffer dielectric layer can be inserted to decouple the heating budget, thus preserving the polymers from carbonization and degassing [Maiolo et al., 2006]. Therefore, this technique can be successfully applied also to ZnO nanostructures manufacturing grown on flexible substrates, even biodegradable ones, to improve the enhancement and the uniformity of the Raman response, simply tuning the morphology of the surface in a convenient way.

In this work, we propose a simple, low-cost and label free biosensing platform based on silver coated ZnO disordered nanostructures (lasered or not) as rapid tool to enhance Raman response from complex organic samples such as whole blood, in order to obtain valuable information without any additional treatment, such as sample purification, separation, etc. This platform could represent a further step to obtain a device to be implemented as potential tool for liquid biopsy [Lone et al., 2022; Ignatiadis et al., 2021]. The usage of laser can allow a scalable method to tailor the surface morphology thus tuning the platform response according to the application. The implementation of a continuous metallic film reduces significantly the potential health issues related to nanoparticles dispersion in the body in case of invasive device procedure, while the application of ZnO as main material ensures the demonstration of an environmental friendly manufacturing process, scalable and easy to transfer to industry, where the metallic film can be recycled once the device has been used. Finally, the implementation of low temperature manufacturing methodologies, open the possibility to utilize also biodegradable substrates to further reduce the environmental impact of the platform.

2. Material and methods

2.1. ZnO nanostructures growth

ZnO nanostructures were grown adopting a scalable and low-cost method called chemical bath deposition (CBD), keeping the working temperature below 85 °C. Two types of substrates were used: a rigid one made in oxidized silicon and a flexible polyimide film (12 μm thick). According to a recipe described in [Fiaschi et al., 2018] disordered hexagonal ZnO nanorods have been obtained with an average size of 100 nm and a length of 800 nm. In case of polyimide substrate, an additional buffer layer (250 nm thick) composed of silicon nitride and silicon oxide has been deposited via plasma enhanced chemical vapor deposition technique (PECVD) at a temperature of 200 °C [Maiolo et al., 2006]. All the manufacturing techniques proposed in this fabrication flowchart are high scalable and potentially applicable to roll-to-roll manufacturing methods.

2.2. XeCl excimer laser annealing and surface characterization

To tune the morphology of the ZnO nanostructures we used a XeCl excimer laser with a wavelength of 308 nm and a Gaussian beam with a rectangular shape of 1 mm × 40 mm. The samples were loaded into a vacuum chamber at an operating pressure of $1x10^{-5}$ mbar without using any additional sample heating; through a stepping motor by Newport we scanned the samples adopting a procedure with 5 shots per point at an operating frequency of 10 Hz. ZnO samples were irradiated with different energy densities, ranging from 50 to 100 mJ/cm^2. The laser annealing modified the surface of the ZnO nanostructures, producing partial or full melting of nanorods tips (see Fig. 1a and b), while for higher energy densities, we observed material flattening and partial ablation. For an accurate analysis of lasered nanostructures see Supplementary Information.

2.3. Sample fabrication

After the ZnO nanorods growth, the biosensing platform was rinsed in deionized water and loaded in a thermal evaporator to deposit silver or gold in a range from 25 to 150 nm (see Fig. 1c). Subsequently, the samples were cut with a dicing saw and cleaned in acetone and deionized water. In case of flexible substrate, samples were cut with scissors (see Fig. 1d). The SERS-like biosensing platform has been tested with silver or gold to evaluate the sample performance.

2.4. Surface characterization and impedance spectroscopy

In case of surface area measurements, the isotherm curves have been obtained equilibrating 200 mg of adsorbent in 100 ml of IPA solution of Methylene Blue (MB) at concentration ranging from 0.02 to 0.001 mg/ml for 24 h at room temperature in dark condition. The determination of the amount of the adsorbed molecules has been performed by the measurement of the residual dye in the solution using a Lambda35 UV–Vis Spectrophotometer. In case of impedance spectroscopy, the samples have been placed in a testing chamber made by Teflon with a gold counter electrode and a platinum reference electrode: we used a 0.9% saline solution as medium and we performed frequency scan up to 4 kHz with a PAR VersaSTAT 4 potentiostat.

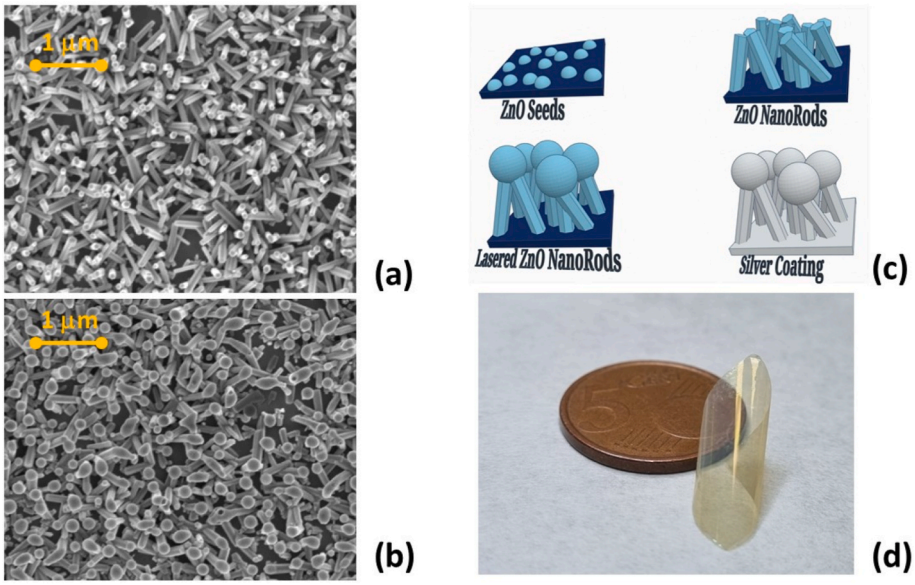

Fig. 1. A SEM imaging of the as deposited sample, showing the ZnO nanorods grown on silicon wafer (a); SEM imaging of the lasered ZnO nanostructures for a sample irradiated at 100 mJ/cm^2 (b); a sketch of the process flow for the fabrication of the lasered Ag/ZnO Raman platform (c); a picture of the lasered ZnO nanorods implemented as Raman platform manufactured on polymeric flexible substrate (d).

2.5. Ex vivo blood specimen collection

The blood samples have been collected during autopsies ordered by the local law enforcement to carry out forensic toxicology investigations and verify possible death-related crimes. Ex vivo sampling has been carried out according to the following protocol. Upon entering the corpse's chest, a small phlebotomy has been performed on the anterior surface of the inferior cava vein. Then, 5 ml of blood has been drawn by a needle-free syringe to minimize the risk of red blood cells' hemolysis. About 1 ml of the blood sample has been slowly dispensed in a plastic tube, which has been closed with a screw-cap and labelled to identify the donor cadaver and the time from death. The fresh blood sample (without anticoagulants) has been stored at −18 °C prior to drop casting on the nanostructured substrate for Raman mapping.

3. Results and discussion

3.1. Nanostructure characterization

To determine the influence of the laser on the nanostructured surface we investigated the biosensing platform through SEM imaging, Surface Area (SA) measurements and Impedance Spectroscopy (see Figs. 1–2). As expected, SEM imaging shows a partial melting of the tips of the nanorods and a redistribution of the material, that decreases its thickness (from 800 to 400 nm), as the laser energy density increases. From previous works we demonstrated that the internal crystalline structures of the nanorods do not change significantly and the composition of the roundish tip is slightly richer in zinc [Carlomagno et al., 2022]. Conversely the effective area and the conductivity of the lasered samples showed a general increase that can be measured by chemical methods and via impedance spectroscopy.

The direct measurement of the SA of the samples has been performed exploiting the principle of dye adsorption. In analogy with the adsorption of N_2 molecules from gas (a.k.a. Brunauer-Emmett-Teller (BET) method) – the standard technique used for nanomaterials [ISO 9277:2010] – we generalized such approach investigating the adsorption isotherms of Methylene Blue (MB) in isopropanol (IPA) [Sørensen and Wakeman, 1996; Kovtun et al., 2019]. This analysis shows an increase of the effective area for the lasered sample of a factor 4 (see supplementary information for details and calculations).

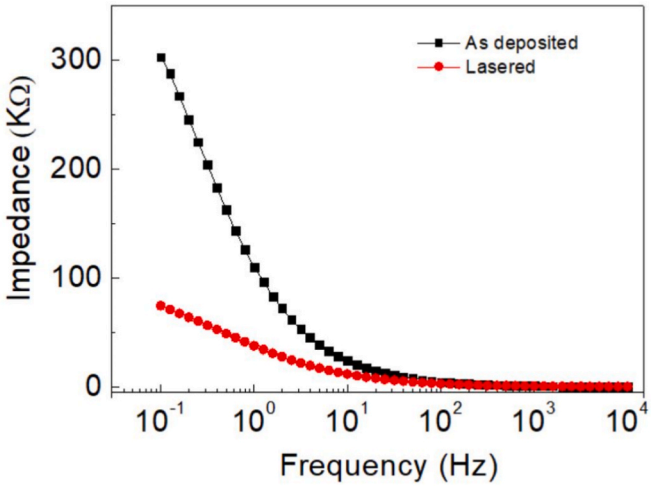

Fig. 2. Impedance spectroscopy analysis for the lasered and the as deposited samples.

A similar indication of the increase of the effective area has been obtained through impedance spectroscopy analysis. As can be noted by Fig. 2 at low frequency the impedance of the as deposited sample increases of 4 times, demonstrating the importance of the laser treatment in providing morphological surface changes and increasing surface uniformity, as demonstrating by the modification of contribution of the constant phase element (CPE) capacitance (see our previous work [Carlomagno et al., 2022]) where a simple Randles model has been adopted to describe the impedance behavior of the samples. These data are in a good agreement, confirming an increment of the surface area of a factor 4 between the surface of the as deposited sample and the lasered one at least at low frequencies. This in turn provides a modification of the surface morphology and an increment in material conductivity that can be very useful to increase the sensitivity of electrochemical based sensors, when the ZnO lasered material is implemented as active sensor material, even if at same time it slightly reduces the Raman response due to the chemical and mechanical interaction between the nanostructured surface and the silver layer.

3.2. Device optimization with rhodamine

To obtain the most efficient Raman biosensing platform, we studied the behavior of the samples with a standard organic dye, rhodamine 6G (RG6) as a target, by using two disordered surface morphologies (as deposited and lasered), different metal coverage (Ag and Au) and different metal thicknesses (from 25 to 200 nm). In particular, a 3 μl drop of a 100 nM RG6 aqueous solution was deposited on the sample platform via drop-casting and dried in air. Raman spectra have been then obtained by means of a DXR2xi Thermo Fisher Scientific Raman Imaging Microscope equipped with a 532 nm excitation source, to exploit the resonance Raman effect associated with the visible absorption of the target dye [Hildebrandt and Stockburger, 1984]. The reported data represent the average of 1900 spectra composing a map of the sample drop collected at 1 mW of laser power. Each point spectrum resulted from 20 accumulations of 20 ms acquisition each. As can been seen from Fig. 3a, the silver coverage provides a significantly higher Raman response respect to the gold one, due to the better tuning of the used 532 nm excitation with the corresponding Surface Plasmon Resonance of the metal. The effect is notable, and even at such low excitation power (1 mW), allows well distinguishing also the less intense vibrational peaks of the studied molecule, such as the band located at about 1433 cm^{-1} which is a quite interesting one being predicted by calculations [Watanabe et al., 2005] but generally visible only for very efficient SERS structures [Hildebrandt and Stockburger, 1984; Watanabe et al., 2005; He et al., 2012].

Moreover, the obtained enhanced intensity has an evident not monotone dependence on the silver layer thickness (see Fig. 3b and c). In particular, for the samples with the as deposited ZnO NRs (Zinc Oxide Nanorods) we observed an initial rapid signal increase, with a maximum Raman enhancement for a silver film thickness of 75 nm (green curve of Fig. 3b), followed by a reduction of the intensity for greater thicknesses. This dependence is well evidenced in the figure inset, presenting the behavior of the single 1650 cm^{-1} peak intensity with the Ag thickness, and is due to the specific SERS mechanism provided by a strict contact between the metallic nanostructures and the target molecule. In fact, very thick metal layers reduce the enhancement effect due to the masking of the underlying nanostructures, so that the substrate gradually tends to behave like a flat surface. However, this thickness dependence appears not uniform along the full spectral range, so that the sample with 100 nm Ag coverage shows a slightly higher signal for the peaks in the range between 600 and 800 cm^{-1} (see red curve Fig. 3b). This peculiar spectral trend can be attributed to a not uniform distribution of the as deposited ZnO nanostructures, and to a multimodal behavior of the RG6 fluorescence that makes its correction by polynomial fitting not uniform on the whole spectral range (see supplementary information).

Conversely, for the lasered ZnO NRs samples, the trend is clearer, showing a maximum of intensity for a 100 nm Ag layer: starting from a 25 nm thick metal layer (black curve), the Raman signal first increases with the silver film thickness, probably due to a better and more uniform metal coverage of the nanostructured substrate. Then, for a 100 nm thick

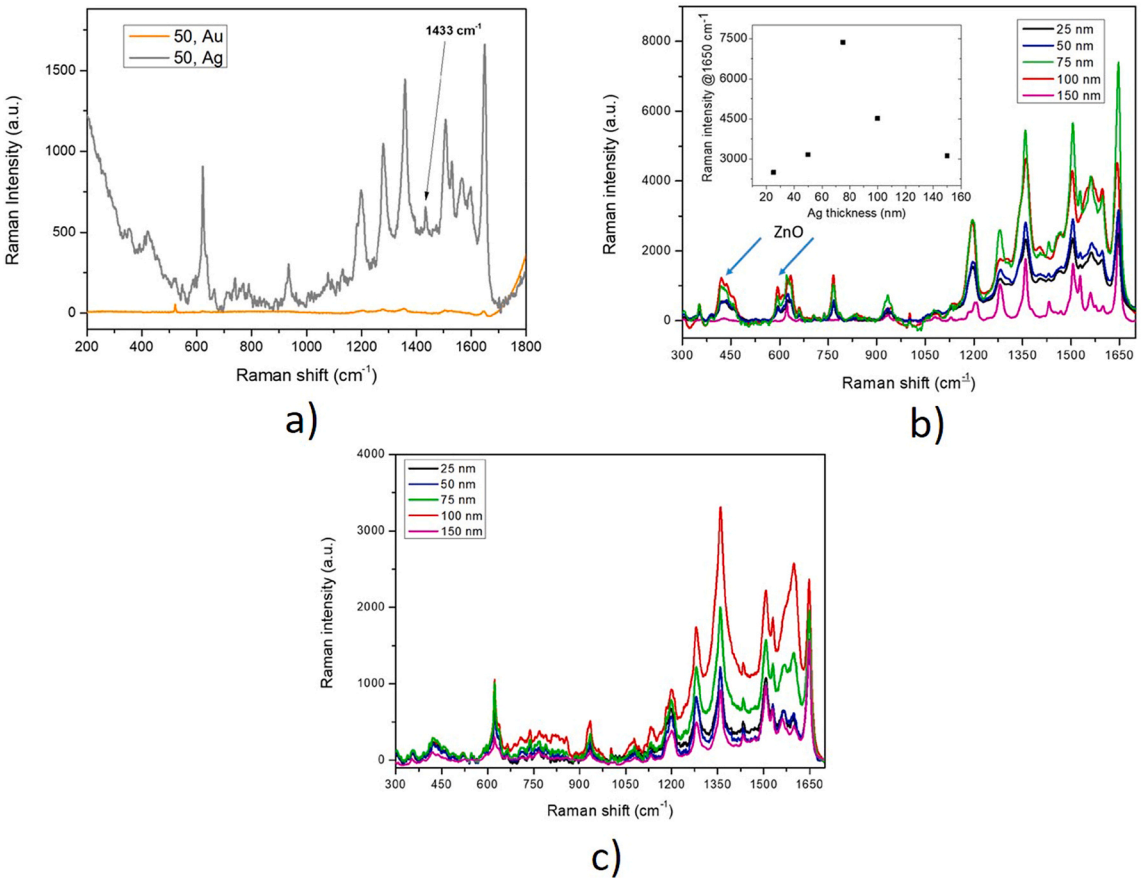

Fig. 3. Comparison of the Raman spectra obtained as the average of the spectral maps acquired on a drop of RG6 solution deposited on a ZnO NRs sample coated with 50 nm of Ag (black line) and Au (orange line) (a); Raman spectra obtained as the average of the spectral maps acquired on a drop of RG6 solution deposited on as deposited Ag/ZnO NRs for different thicknesses of Ag coating; in the inset we report the trend of the Raman response vs the Ag thickness taken at 1650 cm-1 peak to better visualize the result (b); Raman spectra obtained as the average of the spectral maps acquired on a drop of RG6 solution deposited on lasered Ag/ZnO NRs for different thicknesses of Ag coating (c).

Ag layer (red curve), the signal intensity reaches a maximum, to finally decrease following further silver thickening (see the magenta curve corresponding to a 150 nm film). In fact, very thick metal layers reduce the enhancement effect as happens for the as deposited samples. Furthermore, in the lasered samples, the contribution deriving from the zinc oxide layer, indicated by arrows in Fig. 3b, is significantly lower, thus allowing to capture target Raman information also in the range between 350 and 600 cm^{-1}. This behavior can be attributed to an amorphization of the ZnO nanostructures or to the presence of zinc-rich regions on the tips of the structure after the laser treatment.

From this analysis, we can speculate that, although the Raman intensity spectra can be higher for the samples with the as deposited ZnO NRs (see Fig. 3b), the lasered samples have three main advantages: (i) the morphology is more uniform and this is crucial to simplify the data interpretation also for non-expert users; (ii) the correction of the fluorescence background coming from the target by means of polynomial fitting appears to be more effective, due to a monotone signal behavior, which again simplifies the data processing and interpretation; (iii) the Raman signal interference coming from the underlying layer of ZnO is less intense in the lasered samples, allowing the visualization of spectral information also in the region 350-600 cm^{-1}.

3.3. Raman analysis on human blood

Blood plays a fundamental role in a number of life functions and biological activities, thus its qualitative and quantitative analysis represents a common and powerful way to diagnose a wide variety of diseases, monitor the health human status and even carry out forensic investigations at the crime scene. Several analytical techniques have been proposed and used over time to measure whole blood and specific blood components, to control degradation and storage lesions of transfusion products [Delobel et al., 2010], for therapy response assessment [Streitz et al., 2013] and coagulation detection [Tripathi et al., 2017] or to perform "liquid biopsy", thus revealing cancer biomarkers including circulating tumor cell exosomes, tumor DNAs, proteins and non-coding microRNAs [Lone et al., 2022; Ignatiadis et al., 2021]. In this context, Raman spectroscopy represents a strategic tool, because it does not require sample labelling, it is not hindered by water contributions, and potentially allows to recognize single molecular vibrational signatures to identify multiple components also in a complex sample mixture [Atkins et al., 2017; Huang et al., 2022; Zhang et al., 2019]. However, to this aim it is necessary to obtain a sufficiently high and defined signal level, so to consent the distinction of the different contributions and to analyse and compare in detail blood samples.

Here, we tested our Ag/ZnO platform by collecting the Raman spectrum of whole blood and comparing it with the data acquired on a standard glass slide, usually utilized to perform μ-Raman analysis of blood samples, both in diagnostics and forensic applications. The final goal is to verify if the nanostructured substrates can be conveniently proposed as a possible alternative to rapidly obtain good quality spectra of complex biological fluids even by using lower and less destructive laser powers. Therefore, the liquid sample has been dropped on both a lasered ZnO nanostructured substrate covered with 100 nm of silver and a microscope glass slide. Then, Raman maps have been measured after air drying by using identical experimental conditions: 1 mW of Laser power, 20 accumulations of 10 ms acquisition each. Fig. 4 reports the spectra corresponding to the average of the 2000 spectra composing the two maps (black curve on Ag/ZnO, blue curve on glass). The data show a significant intensity increase attained on the nanostructured layer, which permits to well distinguish all the relevant peaks ascribed to haemoglobin and also some interesting spectral contributions that are not visible on the blue spectrum. Among them, the 724 cm^{-1} peak of hypoxanthine [Premasiri et al., 2012], green arrow, the two bands at 917 and 1066 cm^{-1} ascribed to glucose [Azkune et al., 2019], red arrows, and the lipoprotein signatures at 1455 and 1474 cm^{-1} [Koster et al., 2021], magenta arrows. This notable result clearly demonstrates a possible implementation of the proposed platform as potential tool for liquid biopsy and for rapid profiling information.

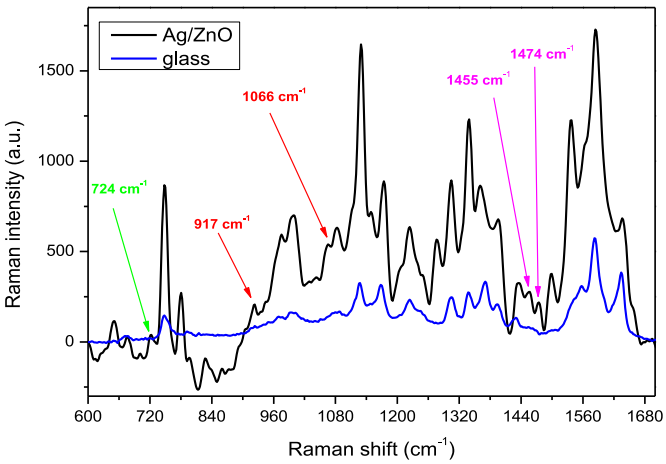

Fig. 4. Comparison of the Raman spectra of an ex vivo human blood sample deposited on glass (blue curve) and on lasered Ag coated ZnO platform. The silver layer has a thickness of 100 nm. The arrows indicate some relevant bands only visible on the nanostructured biosensing platform.

4. Conclusions

In this work a low-cost, label free and low impact Raman biosensing platform, based on Ag coated ZnO NRs, has been characterized and optimized to extract significant information from untreated whole blood sample to propose the device as a rapid diagnostic tool. In particular, the biosensing platform has been deeply investigated varying multiple parameters such as morphology of the nanostructure, type of metal layer (Au or Ag), thickness of the metal coating, etc. To understand which 3D surface can promote the most reliable Raman response, maintaining a sustainable manufacturing process. From this study, lasered ZnO NRs coated with 100 nm thick silver layer achieve a promising SERS-like signal amplification with a less intense ZnO interfering contribution respect the as deposited devices; they also present superior surface properties in terms of effective area (increment of a factor 4), electrical conductivity and sample uniformity, thus opening the possibility to implement the same active material as optical and electrochemical sensor in a multi-purpose configuration. This lasered ZnO nanostructured platform has been tested as fast tool to map complex organic samples like untreated human blood. In particular, data can easily distinguish all the relevant peaks ascribed to haemoglobin even if a very low laser source power (1 mW) is used. Additionally, the response of the lasered Ag/ZnO NRs platform show many other interesting peaks related to hypoxanthine (at 724 cm^{-1}), glucose (917 and 1066 cm^{-1}) and lipoproteins (at 1455 and 1474 cm^{-1}), demonstrating the improved performance of the proposed platform respect of the standard substrates used in forensic studies.

CRediT authorship contribution statement

L. Maiolo: and, Conceptualization, Supervision, Funding acquisition, Validation, Formal analysis, Investigation, Visualization, Writing – original draft, Writing – review & editing. **F. Maita:** Data curation, Investigation, Visualization, Validation, Writing – review & editing. **J.I. Del Rio De Vicente:** Data curation, Investigation, Validation, Writing – review & editing. **I. Lucarini:** Data curation, Investigation, Visualization, Validation, Writing – review & editing. **G. Strisciullo:** Data curation, Validation, Writing – review & editing. **S. Sablone:** Data curation, Validation, Writing – review & editing. **A. Liscio:** Formal analysis, Methodology, Validation, Writing – review & editing. **G. Petrone:** Data curation, Investigation, Validation, Writing – review & editing. **V.**

Mussi: Conceptualization, Supervision, Formal analysis, Investigation, Visualization, Validation, Writing – original draft, Writing – review & editing.

Declaration of competing interest

The authors declare that they have no known competing financial interests or personal relationships that could have appeared to influence the work reported in this paper.

Data availability

Data will be made available on request.

Acknowledgments

This research has been partially supported from the Marie Skłodowska-Curie Innovative Training Network under grant agreement n° 956325 (Astrotech), funded by the European Community's Framework program Horizon 2020. We thank Eleonora Fiorentini for valuable experimental support during her Master Thesis at the Institute for Microelectronics and Microsystems.

Appendix A. Supplementary data

Supplementary data to this article can be found online at https://doi.org/10.1016/j.biosx.2023.100309.

References

Adesoye, S., Dellinger, K., 2022. Sensing and Bio-Sensing Research 37, 1–12, 100499.
Araujo, A., Pimentel, A., Oliveira, M.J., Mendes, M.J., Franco, R., Fortunato, E., Aguas, H., Martins, R., 2017. Flex. Print. Electron 2, 014001.
Atkins, C.G., Buckley, K., Blades, M.W., Turner, R.F.B., 2017. Appl. Spectrosc. 71 (5), 767–793.
Azkune, M., Frosch, T., Arrospide, E., Aldabaldetreku, G., Bikandi, I., Zubia, J., Popp, J., Frosch, T., 2019. J. Lightwave Technol. 37, 2981–2988.
Barveen, N.R., Wang, T.-J., Chang, Y.-H., Yuan-Liu, Z., 2021. J. Alloys Compd. 861, 157952.
Carlomagno, I., Lucarini, I., Secchi, V., Maita, F., Polese, D., Mirabella, S., Franzò, G., Notargiacomo, A., Di Santo, G., Gonzalez, S., Petaccia, L., Maiolo, L., 2022. Appl. Surf. Sci. 587, 152313.
Chen, L.-Y., Yu, J.-S., Fujita, T., Chen, M.-W., 2009. Adv. Funct. Mater. 19, 1221–1226.
Convertino, A., Mussi, V., Maiolo, L., 2016. Sci. Rep. 6, 1–10, 25099.
Daima, H.K., Navya, P.N., Ranjan, S., Dasgupta, N., Lichtfouse, E., 2020. Nanoscience in Medicine, vol. 1. Springer.
Delobel, J., Rubin, O., Prudent, M., Crettaz, D., Tissot, J.-D., Lion, N., 2010. Int. J. Mol. Sci. 11, 4601–4617.
Fiaschi, G., Mirabella, S., Franzò, G., Maiolo, L., Chitu, A., Komem, Y., Shacham-Diamand, Y., 2018. Appl. Surf. Sci. 458, 800–804.
Hakimian, F., Ghourchian, H., Hashemi, H.S., Arazoo, M.R., Rad, M.B., 2018. Sci. Rep. 8, 1–9, 2943.
He, X.N., Gao, Y., Mahjouri-Samani, M., Black, P.N., Allen, J., Mitchell, M., Xiong, W., Zhou, Y.S., Jiang, L., Lu, Y.F., 2012. Nanotechnology 23, 205702.
Hildebrandt, P., Stockburger, M., 1984. J. Phys. Chem. 88, 5935–5944.
Huang, S.-J., Chiang, C.-C., Immanuel, P.N., Subramania, M., 2022. Coatings 12, 893.
Huang, J., Chen, F., Zhang, Q., Zhan, Y., Ma, D., Xu, K., Zhao, Y., 2015. ACS Appl. Mater. Interfaces 7, 5725–5735.
Ignatiadis, M., Sledge, G.W., Jeffrey, S.S., 2021. Nat. Rev. Clin. Oncol. 18, 297–312.
ISO 9277:2010, 2010. "Determination of the Specific Surface Area of Solids by Gas Adsorption — BET Method" - ICS :19.120 Particle Size Analysis. Sieving.
Korani, M., Ghazizadeh, E., Korani, S., Hami, Z., Mohammadi-Bardbori, A., 2015. Eur. J. Nanomed. 7 (1), 51–56.
Koster, H.J., Rojalin, T., Powell, A., Pham, D., Mizenko, R.R., Birkeland, A.C., Carney, R. P., 2021. Nanoscale 13, 14760.
Kovtun, A., Zambianchi, M., Bettini, C., Liscio, A., Gazzano, M., Corticelli, F., Treossi, E., Navacchia, M.L., Palermo, V., Melucci, M., 2019. Nanoscale 11, 22780–22787.
Kuslich, C.D., Chui, B., Yamashiro, C.T., 2018. Current Protocols Essential Laboratory Techniques e27.
Lee S, S., Choi, I., 2019. BioChip J 13, 30–42.
Leonardi, A.A., Lo Faro, M.J., Petralia, S., Fazio, B., Musumeci, P., Conoci, S., Irrera, A., Priolo, F., 2018. ACS Sens. 3, 1690–1697.
Li, J., Yan, H., Tan, X., Lu, Z., Han, H., 2019. Anal. Chem. 91 (6), 3885–3892.
Lone, S.N., Nisar, S., Masoodi, T., Singh, M., Rizwan, A., Hashem, S., El-Rifai, W., Bedognetti, D., Batra, S.K., Haris, M., Bhat, A.A., Macha, M.A., 2022. Mol. Cancer 21, 79.
Mai, Q.M., Nguyen, H.A., Phung, T.L.H., Dinh, N.X., Tran, Q.H., Doan, T.Q., Pham, A.T., Le, A.-T., 2022. ACS Appl. Nano Mater. 5 (10), 15518–15530.
Maiolo, L., Pecora, A., Fortunato, G., Young, N.D., 2006. J. Vac. Sci. Technol. 24, 280–285.
Mei, R., Wang, Y., Liu, W., Chen, L., 2018. ACS Appl. Mater. Interfaces 10 (28), 23605–23616.
Pecora, A., Maiolo, L., Cuscunà, M., Simeone, D., Minotti, A., Mariucci, L., Fortunato, G., 2008. Solid State Electron. 52, 348–352.
Premasiri, W.R., Lee, J.L., Ziegler, L.D., 2012. J. Phys. Chem. B 116, 9376–9386.
Privitera, V., Scalese, S., La Magna, A., Pecora, A., Cuscunà, M., Maiolo, L., Minotti, A., Simeone, D., Mariucci, L., Fortunato, G., Caristia, L., Mangano, F., Di Marco, S., Camalleri, M., Ravesi, S., Coffa, S., Grimaldi, M.G., De Bastiani, R., Badalà, P., Bagiante, S., 2008. J. Electrochem. Soc. 155 (Issue 10), H764–H770.
Proniewicz, E., Tata, A., Wojcik, A., Starowicz, M., Pacek, J., Molenda, M., 2020. Phys. Chem. Chem. Phys. 22, 28100–28114.
Raveendran, J., Stamplecoskie, K.G., Docoslis, A., 2020. ACS Appl. Nano Mater. 3 (3), 2665–2679.
Seo, S., Chang, T.-W., Liu, G.L., 2018. Sci. Rep. 8, 1–11, 3002.
Sørensen, B.L., Wakeman, R.J., 1996. Water Res. 30 (Issue 1), 115–121.
Streitz, M., Miloud, T., Kapinsky, M., Reed, M.R., Magari, R., Geissler, E.K., Hutchinson, J.A., Vogt, K., Schlickeiser, S., Handrup Kverneland, A., Meisel, C., Volk, H.-D., Sawitzki, B., 2013. Transplant. Res. 2 (17), 1–15.
Sun, Q., Zhang, Q.Y., Zhou, N., Zhang, L.Y., Hu, Q., Ma, C.Y., Zhang, C., Yi, Z., 2020. Appl. Surf. Sci. 526, 146565.
Syedmoradi, L., Daneshpour, M., Alvandipour, M., Gomez, F.A., Hajghassem, H., Omidfar, K., 2017. Biosens. Bioelectron. 87 (15), 373–387.
Tan, E.-Z., Yin, P.-G., You, T.-T., Wang, H., Guo, L., 2012. ACS Appl. Mater. Interfaces 4 (7), 3432–3437.
Tang, J., Xiong, L., Wang, S., Wang, J., Liu, L., Li, J., Yuan, F., Xi, T., 2009. J. Nanosci. Nanotechnol. 9 (8), 4924–4932.
Tran, D.T., Nguyen, T.H., Nguyen, T.B., 2022. J. Raman Spectrosc. 53 (6), 1039–1047.
Tripathi, M.M., Egawa, S., Wirth, A.G., Tshikudi, D.M., Van Cott, E.M., Nadkarni, S.K., 2017. Sci. Rep. 7 (9169), 1–8.
Watanabe, H., Hayazawa, N., Inouye, Y., Kawata, S., 2005. J. Phys. Chem. B 109, 5012–5020.
Williams, R.M., Lee, C., Galassi, T.V., Harvey, J.D., Leicher, R., Sirenko, M., Dorso, M.A., Shah, J., Olvera, N., Dao, F., Levine, D.A., Heller, D.A., 2018. Sci. Adv. 4 (4), eaaq1090.
Zhang, Y., Mi, X., Tan, X., Xiang, R., 2019. Theranostics 9 (2), 491–525.
Zhu, Q., Xu, C., Wang, D., Liu, B., Qin, F., Zhu, Z., Liu, Y., Zhao, X., Shi, Z., 2019. J. Mater. Chem. C 7, 2710.